Evaluation of Boundary-Layer Effects in Shock-Tube Studies of Chemical Kinetics

NOBUYUKI FUJII, MITSUO KOSHI, HIROMITSU ANDO, and TETSURO ASABA

Department of Reaction Chemistry, University of Tokyo, Bunkyo-ku, Tokyo, Japan 113

Abstract

Particle times of flight in incident shock flow were determined experimentally by marking several positions of the test gas (mainly Ar) in the shock tube with an infrared emitting gas (NO or CO_2). From the local particle velocity, derived from the particle flight times, temperature and pressure changes behind the shock front were evaluated. Several experimental data were found to be correctly described by Mirels's formulations when used properly. The limitations of the formulations are discussed. It is found to be advisable to evaluate boundary-layer effects on shock-tube flow by experiments, rather than theory, in carrying out chemical kinetics studies.

Nomenclature and Subscripts

Nomenclature

A	cross-sectional area (see Fig. 7)
M_2	Mach number in region 2 relative to shock front
M_s	shock Mach number
Re	Reynolds number
T	temperature
U_s	shock velocity
a	sound velocity
l	distance behind shock front, $t_l \cdot U_s$ (see Fig. 2)
p	pressure
t_f	particle time of flight (see Fig. 2)
t_l	laboratory particle time of flight (see Figs. 1 and 2)
u_2	particle velocity relative to shock velocity
x	distance from observation station (see Fig. 2)
γ	specific heat ratio
μ	viscosity coefficient

International Journal of Chemical Kinetics, Vol. XI, 285–304 (1979)

0538-8066/79/0011-0285$01.00

ρ density
ρ_{21} density ratio across shock, ρ_2/ρ_1
τ test time, that is, period between arrival of shock front and that of contact surface at the station (see Fig. 1)

Subscripts

1 region before shock front (see Fig. 2)
2 region behind shock front (see Fig. 2)
i inviscid flow (see Fig. 2)
s immediately behind shock front
t transition from laminar to turbulent (see Figs. 1 and 7)
lam laminar (see Fig. 7)
turb turbulent (see Fig. 7)
m maximum separation

Introduction

Although numerous chemical kinetics studies have been performed using shock tubes, which are considered irreplaceable tools in high-temperature studies, it is felt that the kinetic parameters obtained from shock tubes are sometimes treated as less credible than those from other techniques, such as flow reactors and closed vessels. This is perhaps mainly due to the ambiguity in evaluating shock-flow parameters indirectly from the shock velocity, since in the study of chemical kinetics it is essential to know exactly the conditions under which reaction takes place, for example, temperature, time, and concentration of reactants and/or products.

It is well recognized that actual shock parameters deviate from those evaluated by the inviscid, constant-area flow model due to the effects of the wall boundary layer. Accordingly, there have been many studies of boundary-layer effects on the nature of the core flow in shock tubes. Among them, Mirels's extensive formulations [1] of the effects have been referred to by several investigators in shock-tube studies of chemical kinetics [2]. It is considered, however, that there are several problems left when applying his formulations to the practical kinetic study. (a) Transition of the boundary-layer flow from laminar to turbulent often takes place, but Mirels's formulations do not apply in this case; (b) although there is a Mirels's criterion for the condition of the transition, that is, a transition Reynolds number [3], it seems to be questionable; (c) the similarity parameters adopted by Mirels are not so credible for the case of turbulent boundary layers (this was pointed out by several researchers [4] based on their experiments); (d) Mirels's formulations are derived for the case of the "limiting flow condition," and no verification is presented for the preliminiting flow condition.

In this paper we describe a new empirical method for evaluating the boundary-layer effects on core flow properties. This method has several advantages as follows. (a) Since the particle time of flight is obtained directly from experiments, one can learn the exact reaction time. The procedure is considered to be the best way for the study of chemical kinetics. (b) From the data thus obtained, the profiles of temperature and pressure can be derived using Mirels's formulation. (c) The method described here is better than the measurement of the test time, that is, the period between arrival of the shock front and that of the contact surface at the observation station, since the latter is affected irregularly by the nonideal performance of diaphragm rupture.

Correcting the shock-tube data by this method, it is expected that kinetic parameters obtained by shock tubes are considered to be as reliable as those obtained by any other techniques.

Experimental

Two shock tubes of 5-cm internal diameter, 3.5–6.5 m test section, and 2-m driver section were used. Data obtained by two shock tubes were found to be essentially the same. The observation station was equipped to monitor infrared emission, pressure profile, and heat transfer to a thin-film gauge. Several inlets for tracer gas for measuring the particle time of flight and piezoelectric gauges for measuring the shock velocity were located between 0.5 and 3.6 m upstream of the observation station.

Various gases were used as test gases. Their specific heat ratios, sound velocities, and viscosity coefficients are listed in Table I. Experimental conditions were p_1 = 2–150 torr and M_s = 3–7. NO or CO_2 was used as the tracer gas.

After filling the tube with test gas, a small amount of tracer gas was introduced into the tube from the inlets. The shock wave was generated immediately after the injection of tracer gas. Hydrogen was used as driver gas. The arrival of the tracers at the observation station could be detected

TABLE I. Specific heat ratio γ, sound velocity a, and viscosity coefficient μ of test-gas mixtures at 300 K.

test gas composition	γ	a (m/sec)	$\mu \times 10^7$ [a] (poise)	symbol in Fig. 5
Ar	1.667	322	2217	○
0.5 N_2 + 0.5 Ar	1.5	332	1973	⊙
N_2	1.4	353	1728	●
0.3 He + 0.7 Ar	1.667	378	2134	□
0.06 C_6H_6 + 0.94 Ar	1.5	298	2128	△
0.12 C_6H_6 + 0.88 Ar	1.4	280	2040	▲

[a] Additional law was assumed.

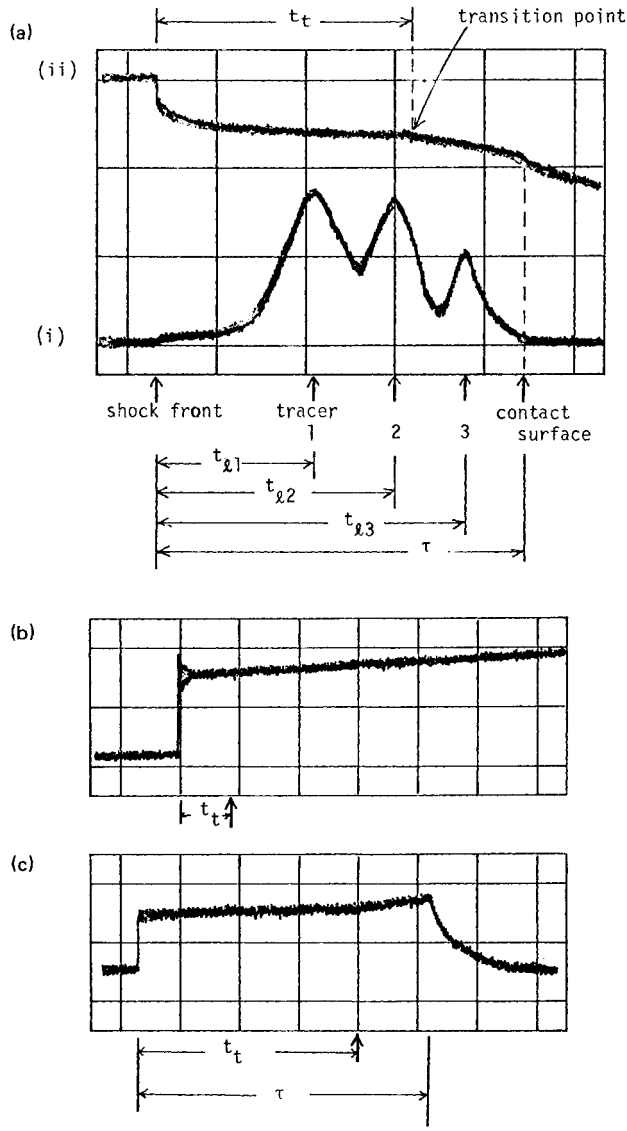

Figure 1. Examples of oscillograms. (a) (i)—signals of tracer gases introduced from three inlets located 1.3, 2.3, and 3.6 m upstream of the observation station, respectively; (ii)—profile of heat transfer to thin film gauge. The inflection point on the profile at t_t from the shock front shows the transition from laminar to turbulent. Test gas is argon; p_1 = 4 torr; M_s = 5.3; 1 division = 100 μsec. (b) Pressure profile. Test gas is argon; p_1 = 150 torr; M_s = 4.3; 1 division = 100 μsec. Transition point is obtained by calculation. (c) Infrared emission of nitric oxide in the case of nitric oxide–argon mixture as test gas. p_1 = 23 torr; M_s = 4.28; 1 division = 100 μsec. Transition point is obtained by calculation.

by monitoring the infrared emission. An example of profiles of tracer-gas emission is shown in Figure 1(a). Since the ratio of concentration of tracer gas to that of test gas at the peak of infrared emission was 0.5–2.0%, the effect on the test-gas properties of introducing the tracer gas was negligible.

Also pressure and temperature profiles were measured piezoelectrically and infrared spectrophotometrically, respectively. Examples of these profiles are shown in Figure 1(b) and (c).

Results and Discussions

Particle Time of Flight

Determination of the time of flight by the tracer method. In Figure 2 the motion of the shock wave is illustrated by an x–t diagram. One can obtain t_1, that is, the laboratory fixed particle time of flight, directly from the tracer experiments. Previous investigators usually used test times τ only for studying boundary-layer effects in shock tubes. The test time is, however, affected by the unideal rupture of the diaphragm, and its exact determination in oscillograms is quite difficult. The tracer method used in this study is free from these ambiguities.

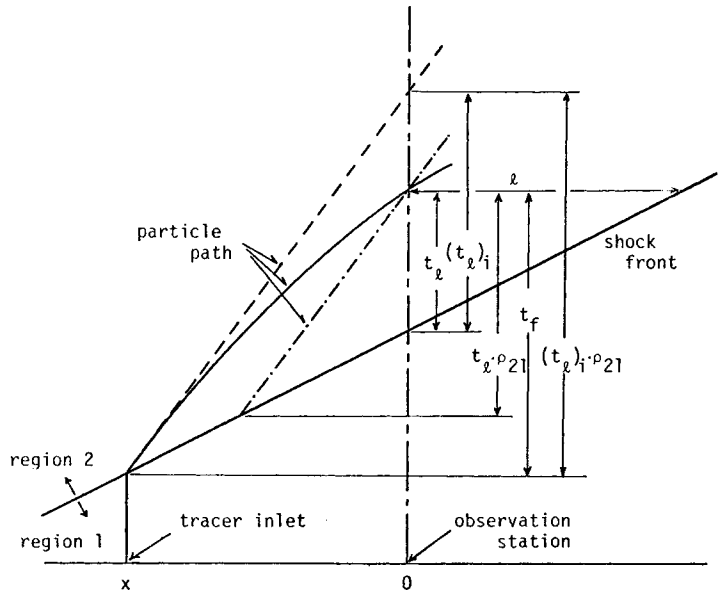

Figure 2. x–t shock diagram in laboratory fixed coordinate system. Particle traces are shown as follows: full line—real case; dashed line—inviscid case; chain line—trace obtained from t_1 assuming inviscid flow.

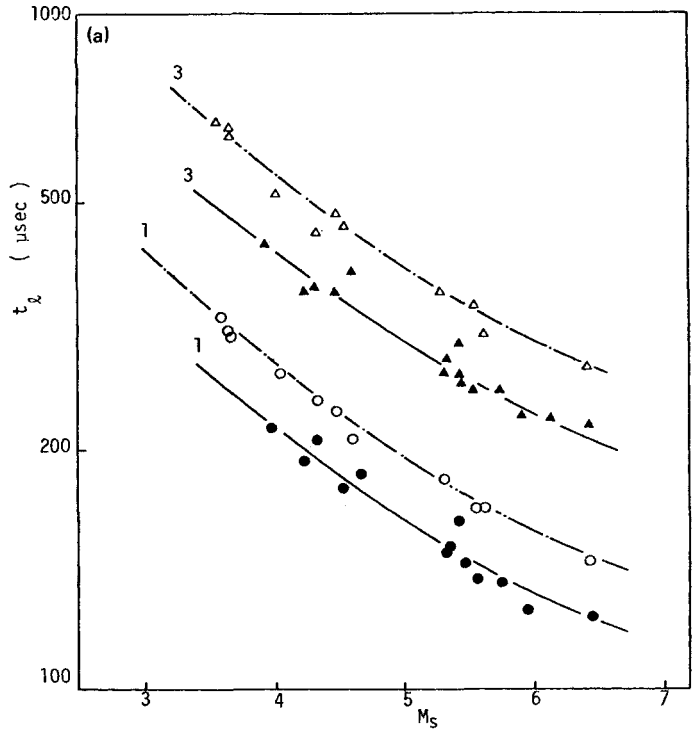

Figure 3. t versus M_s. Test gas is argon. Numbers and marks show the initial position of tracer gases. 1, O—x = 1.3 m; 3, Δ—x = 3.6 m. (a) ●, ▲—p_1 = 2 torr; O, Δ—p_1 = 4 torr. Lines are calculated by Mirels's laminar model: solid lines—p_1 = 2 torr; chain lines—p_1 = 4 torr. (b) O, Δ—p_1 = 10 torr; ⊕, ▲—p_1 = 30 torr; ⊖, ▲—p_1 = 50 torr; ●, ▲—p_1 = 150 torr. Lines are calculated by Mirels's turbulent model: solid lines—p_1 = 10 torr; chain lines—p_1 = 30 torr; dashed lines—p_1 = 150 torr.

Most experiments to investigate boundary-layer effects were carried out using pure argon test gas. As can be seen later, one can apply the results on pure argon to the case of other gases. In Figure 3 t_l values obtained experimentally are plotted against Mach shock numbers. It should be noted that in the case where p_1 is larger than 10 torr, t_l is independent of p_1 within the experimental scatter, in contradiction to Mirels's prediction, and much greater than predicted.

From t_l thus obtained, the particle time of flight t_f can be derived as

$$t_f = t_l + \int_0^x \frac{dx}{U_s} \tag{1}$$

One can obtain t_f correctly from t_l, using the calibration curve of t_f versus t_l similar to curve C in Figure 4. Thus in this treatment it is not necessary

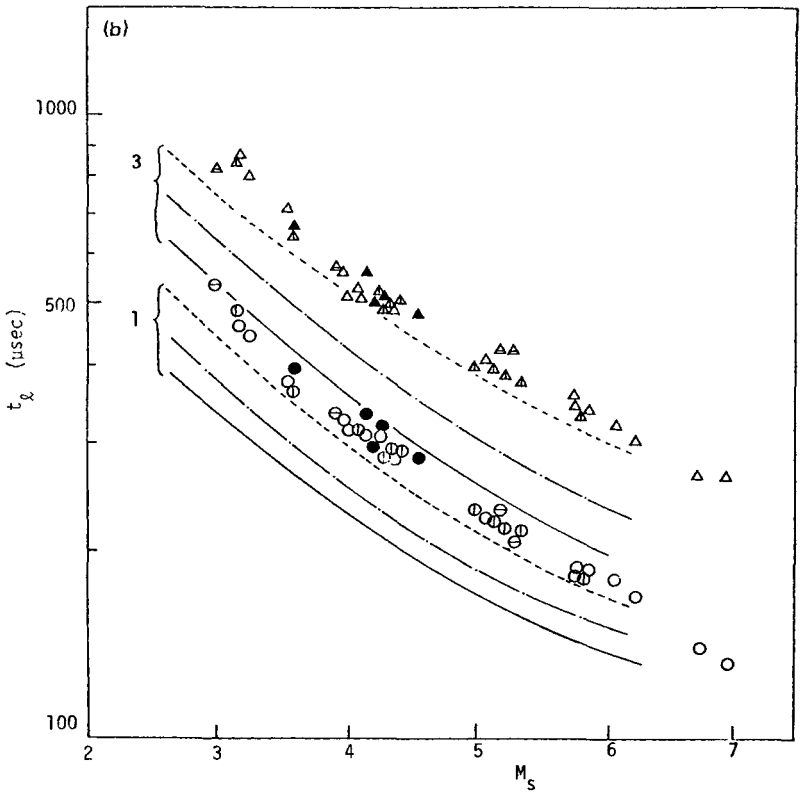

Figure 3. *(Continued from previous page.)*

to consider whether the attenuation of shock velocity is negligible or not. Generally, however, the effect of shock attenuation on the particle time of flight is small or within the scattering of data in conventional shock-tube experiments, including the present work. Then eq. (1) can be converted to

$$t_f \simeq t_l + \frac{x}{U_s}. \tag{2}$$

Application of pure argon results to other test gases. In actual experiments, test-gas mixtures must be handled instead of pure argon. Several gas mixtures (Table I) were examined as test gases. Values of t_l were measured for $p_1 = 20$ Torr.

In the inviscid flow case, $(t_l)_i$ was expressed as

$$(t_l)_i = \frac{x}{M_s a(\rho_{21} - 1)} \tag{3}$$

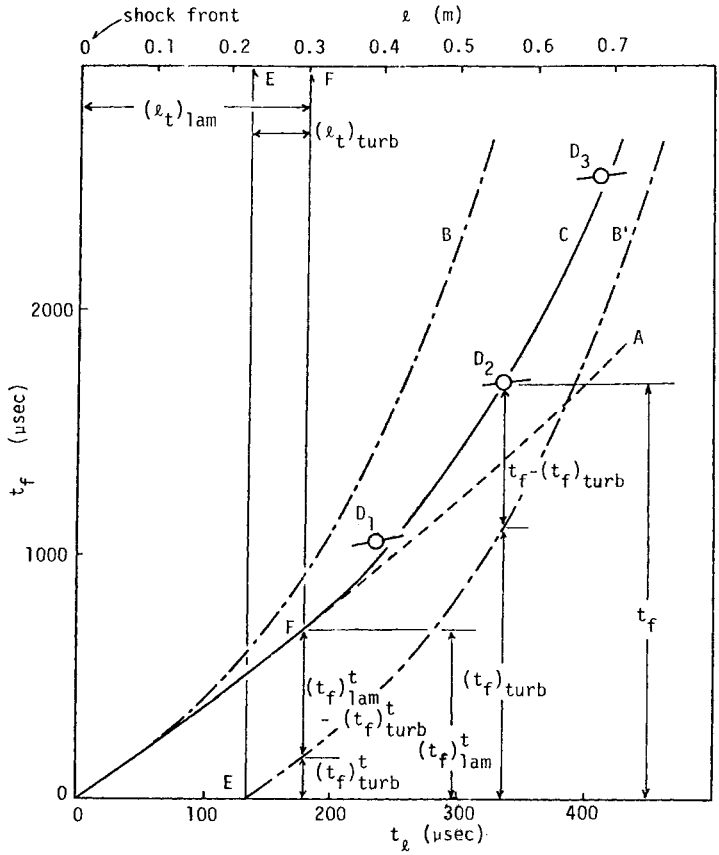

Figure 4. Particle time of flight in the transition case. Test gas argon; $p_1 = 30$ torr; $M_s = 5$. Circles are experimental values; lines are calculated values. A—fully laminar; B—fully turbulent; B'—transposed curve of B; C—transition case; E—effective origin of turbulence; F—transition point.

as shown in Figure 2. Putting α_x as

$$\alpha_x = t_1/(t_1)_i \tag{4}$$

one could obtain the following expression:

$$t_1 = \alpha_x \frac{x}{M_s} \frac{1}{a(\rho_{21} - 1)} \tag{5}$$

When experimental data were put into eq. (5), α_x was found to be approximately independent of the test gas used if M_s and x were fixed, as shown in Figure 5. This is reasonable according to the following considerations. The boundary-layer equations behind the shock front [5] are

$$\frac{\partial(\rho u_{wall})}{\partial x} + \frac{\partial(\rho v_{wall})}{\partial y} = 0 \tag{6}$$

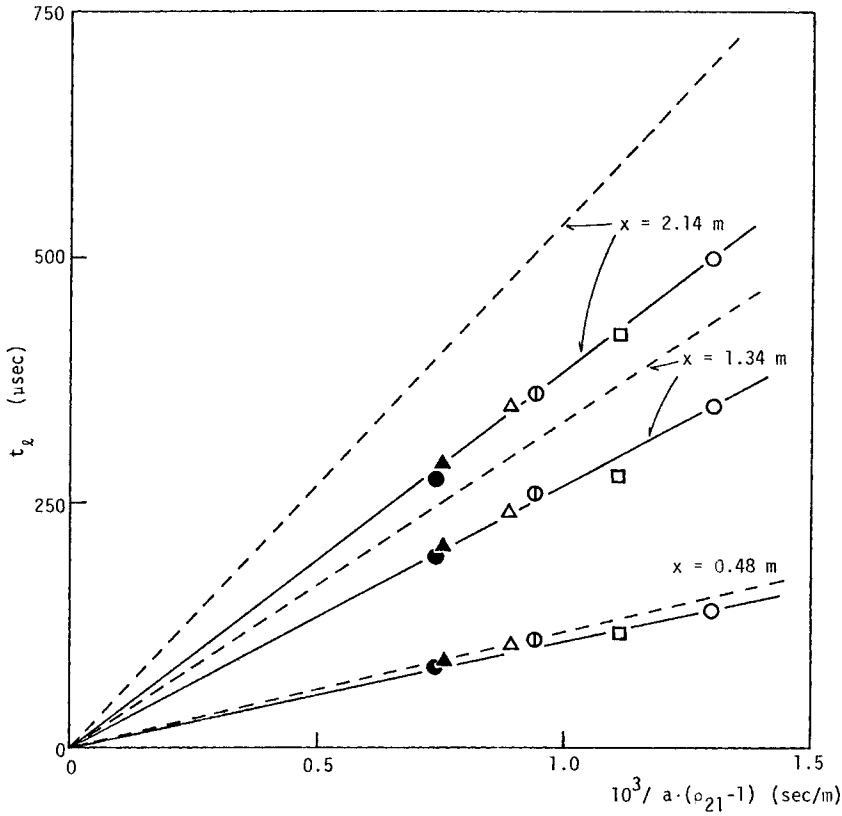

Figure 5. t_1 of various test gases. $p_1 = 20$ torr; $M_s = 4$. Marks are experimental values listed in Table I; dashed lines—inviscid relation $(t_1)_i = x/aM_s(\rho_{21} - 1)$; solid lines—relation $t_1 = \alpha_x x/aM_s(\rho_{21} - 1)$.

$$\rho u_{\text{wall}} \frac{\partial u_{\text{wall}}}{\partial x} + \rho v_{\text{wall}} \frac{\partial u_{\text{wall}}}{\partial y} = \frac{\partial}{\partial y}\left(\mu \frac{\partial u_{\text{wall}}}{\partial y}\right) \tag{7}$$

$$\rho u_{\text{wall}} \frac{\partial H}{\partial x} + \rho v_{\text{wall}} \frac{\partial H}{\partial y} = \frac{\partial}{\partial y}\left(\frac{\mu}{\sigma}\frac{\partial H}{\partial y}\right) + \frac{\partial}{\partial y}\left(\frac{\mu}{2}\left(1 - \frac{1}{\sigma}\right)\frac{\partial u^2_{\text{wall}}}{\partial y}\right) \tag{8}$$

where H is the local stagnation enthalpy, u_{wall} and v_{wall} are the velocities parallel to the x and y axes fixed to the wall of the tube, and μ and σ are the viscosity coefficient and Prandtl number of the test gas, respectively. In the inviscid case, the right-hand sides of eqs. (7) and (8) and the second terms of the left-hand sides of eqs. (6)–(8) are zero, and the solution of the partial differential equation is

$$u_{\text{wall}} = \frac{a(\rho_{21} - 1)}{\rho_{21}} M_s \tag{9}$$

Obviously eq. (3) is equivalent to eq. (9) and is valid regardless of the kind

of gas, as shown in Figure 5. In the viscid case, on the other hand, in order to compare the boundary-layer effects in the various test gases, the partial differential equations must be solved under the boundary conditions expressed by eq. (9) at $x = 0$. In gaseous mixtures, however, the Prandtl number can be approximated as unity, and viscosity coefficients are small and not much different among the test gases, as shown in Table I. Accordingly, the boundary-layer effects on t_1 are also not much different and the α_x values are almost constant, regardless of the kind of gas, at constant Mach numbers.

Experimentally obtained values of α_x $(= t_1/(t_1)_i)$ are shown in Figure 6. If values of α_x for argon are found, as described above, then it is possible to make boundary-layer corrections of the reaction time of other test gases by using the relation

$$t_f \simeq t_1 + \frac{x}{U_s} = [1 + (1/\alpha_x)(\rho_{21} - 1)]t_1 \tag{10}$$

Comparison of experimental results with Mirels's theory. We wish now to compare measured t_1 values with the values calculated by Mirels's formulation. When p_1 is lower than 10 torr, t_1 is in agreement with calculation within the experimental scatter, as shown in Figure 3(a). In this case the

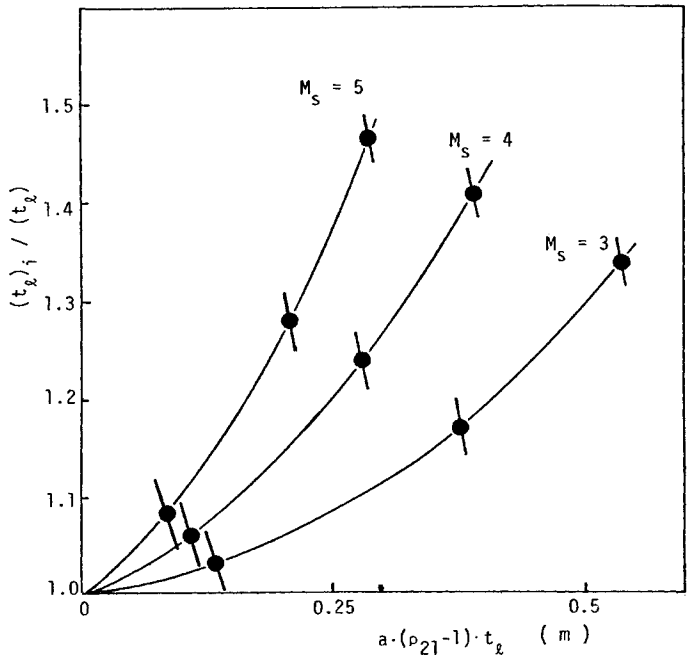

Figure 6. $(t_1)_i/t_1$ versus $a(\rho_{21} - 1)t_1$ of various gases at $p_1 = 20$ torr. Marks show experimental values.

boundary layer could be treated as fully laminar, judging from the heat gauge experiments.[1] On the contrary, when p_1 is higher than 10 torr, the measured values deviate from the calculated values, if it is assumed that fully turbulent boundary-layer flow exists, as shown in Figure 3(b). Since in this case it is reasonably considered that the transition from laminar to turbulent occurs in the boundary layer, one can explain the experimental results as follows.

Mirels presented a variable-area model assuming that the core flow enclosed by the boundary layer is a uniform free stream. In the limiting condition, the contact surface has zero velocity relative to the shock front, and both move with the same velocity separated by a constant distance, the maximum separation length l_m. In Mirels's model $t_f/(t_1\rho_{21})$ can be calculated corresponding to l/l_m, where l is obtainable from $l = t_1 \times U_s$, as shown in Figure 2.

As shown in Figure 7, the axial variation of the cross-sectional area is expressed as

$$A_{2,s}/A_2 = 1 - (l/l_m)^{1-n} \tag{11}$$

Here $n = 1/2$ for laminar and $1/5$ for turbulent.

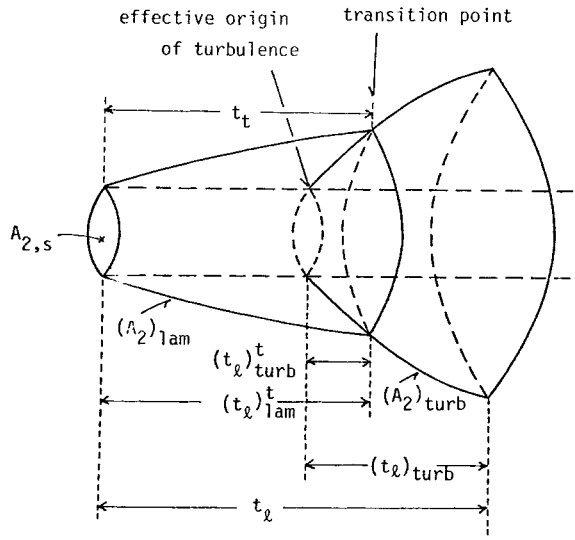

Figure 7. Illustration of the boundary-layer transition from laminar to turbulent by the diverging duct model.

[1] Figure 9 shows that a transition from laminar to turbulent flow occurs in the boundary layer even when p_1 is less than 10 torr. This is also seen in Figure 1(a). In these low-pressure cases, however, the turbulent boundary-layer region occurs so late in the flow that it does not affect t_1 or t_f significantly.

Since all flow properties must be continuous at the transition point, the cross-sectional areas of two diverging ducts are equal, that is, at the transition point,

$$\left(\frac{l_t}{l_m}\right)_{lam}^{1/2} = \left(\frac{l_t}{l_m}\right)_{turb}^{4/5} \tag{12}$$

When $t_t = (t_l)^t_{lam} < t_l$, as shown in the figure,

$$t_l = (t_l)^t_{lam} + (t_l)_{turb} - (t_l)^t_{turb} \tag{13}$$

Using eq. (2),

$$t_f = \begin{cases} (t_f)_{lam}, & t_l < t_t \quad (14a) \\ (t_f)^t_{lam} + (t_f)_{turb} - (t_f)^t_{turb}, & t_l > t_t \quad (14b) \end{cases}$$

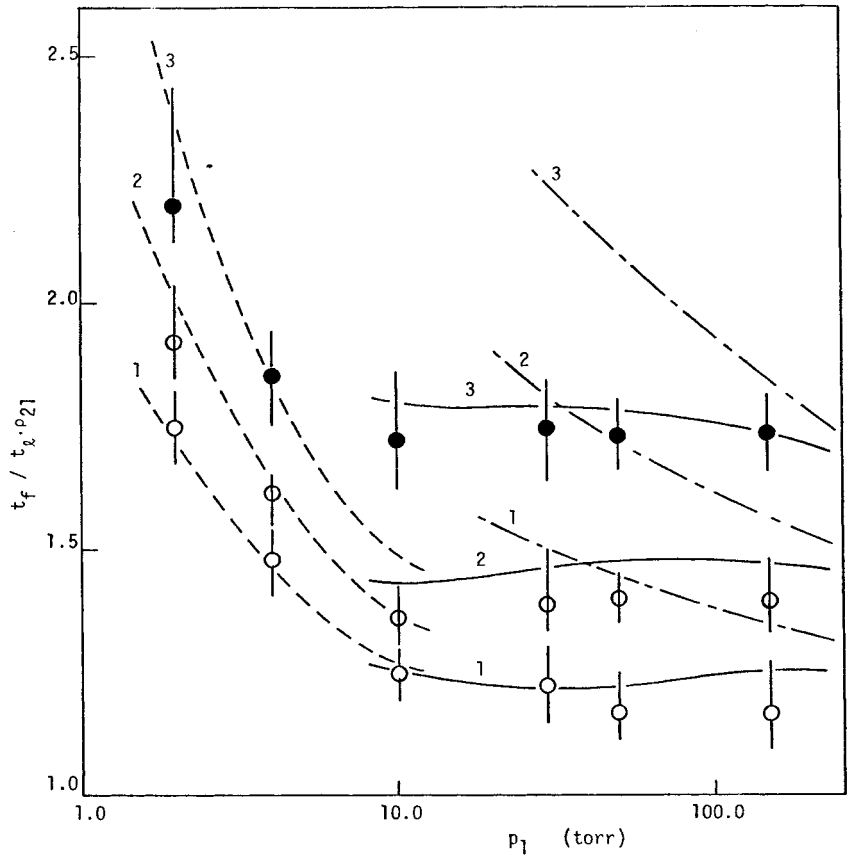

Figure 8. Boundary-layer effects on particle time of flight in argon at $M_s = 4$. Numbers and marks show the initial position of tracer gases: 1, ○—x = 1.3 m; 2, ⊙—x = 2.3 m; 3, ●—x = 3.6 m. Lines—calculated: dashed lines—laminar model; chain lines—turbulent model; solid lines—transition model.

where the superscript t denotes the time required for the particle to travel from the shock front to the transition point in the duct, and subscripts lam and turb denote the laminar and turbulant conditions, respectively.

The procedure for calculating t_f in the case where the transition of the boundary layer occurs is illustrated using Figure 4. (a) A fully laminar curve A, calculated from Mirels's formulation, is drawn from the shock front. (b) A fully turbulent curve B, also calculated from Mirels's formulation, drawn from the shock front, is moved to B′ to obtain the effective origin of turbulence. (c) Choosing a point (for example, D_2), determined by a tracer experiment in which t_f is longer than that calculated by the laminar model, (that is, line A), one can obtain $t_f - (t_f)_{turb}$ from the figure. (d) If line B′ is correctly positioned,

$$t_f - (t_f)_{turb} = (t_f)^t_{lam} - (t_f)^t_{turb} \tag{14'b}$$

should be satisfied, from eq. (14b). So one designates the provisional transition point on curve A, using the relation of eq. (14′b). (e) At the transition point eq. (12) must be satisfied. Here $(l_t)_{lam}$ and $(l_t)_{turb}$ can be obtained as illustrated in the figure, and l_m can be found from Mirels's formulation for the laminar and turbulent cases. (f) One repeats this procedure until eq. (12) is satisfied. (g) After the correct transition point is determined, one can obtain curve C by using D_2, positioned correctly, and eq. (14′b). (h) In the same way one can get the optimum transition point and line C by using other experimental points, such as D_1, D_3, etc. Figure 8 shows examples of the results of such calculations, where the ordinate is normalized by $t_1 \cdot \rho_{21}$ (see also Fig. 2).

From the transition point thus calculated, one can obtain the transition Reynolds numbers [6]:

$$\mathrm{Re}_t = \rho_{2,s} \frac{(U_s - u_{2,s})^2}{\mu_{2,s}} \cdot \frac{U_s}{u_{2,s}} \cdot t_t \tag{15}$$

They are shown in Figure 9 with the values obtained by the heat-gauge experiment. In this experiment it is difficult to distinguish the transition point when p_1 is higher than 10 torr. The experimental Re_t data are not inconsistent with the values calculated from the data of the tracer experiments using the model presented here in which two ducts corresponding to laminar and turbulent boundary layers are connected. It should be noted, however, that Mirels derived transition Reynolds numbers [1] which are independent of p_1, as shown in Figure 9.

Temperature and Pressure Rise Behind Shock Front

Determination of temperature and pressure profiles. It is well known that boundary-layer growth causes the temperature and pressure of the shocked gas to increase gradually behind the shock front. This is evaluated

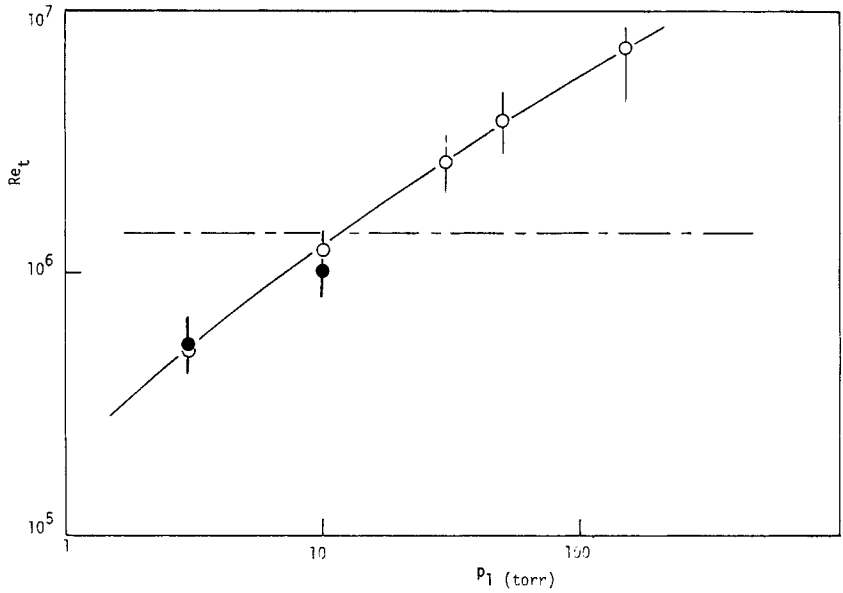

Figure 9. Transition Reynolds number versus initial pressure. ●—values obtained by heat transfer gauge; ○—values calculated from particle time of flight by duct flow model. Chain line shows the value presented by Mirels.

from the data of the tracer experiments as follows. Assuming isentropic flow and constant γ_2 in the flow behind the shock front, the temperature, pressure, and density changes can be calculated from

$$M_{2,s} = \left\{\frac{(\gamma_2 - 1)M_s^2 + 2}{2\gamma_2 M_s^2 - \gamma_2 + 1}\right\}^{1/2} \tag{16}$$

$$\frac{T_2}{T_{2,s}} = \left(\frac{P_2}{P_{2,s}}\right)^{(\gamma_2-1)/\gamma_2} = \left(\frac{\rho_2}{\rho_{2,s}}\right)^{\gamma_2-1} = \frac{2 + (\gamma_2 - 1)M_{2,s}^2}{2 + (\gamma_2 - 1)M_2^2} \tag{17}$$

where $M_2 = u_2/a_2$, $M_{2,s} = u_{2,s}/a_{2,s}$, and the subscript s denotes the condition immediately behind the shock front. Knowing M_s, one calculates $M_{2,s}$ from eq. (16). By using eq. (17), T_2, M_2, P_2, and ρ_2 can be calculated from experimentally determined u_2. Here $u_2 = dl/dt_f$ can be obtained from the gradient of the curve of t_f plotted against l. In Figure 10 examples of profiles of particle velocity relative to shock front, temperature, and pressure thus obtained are shown.

Comparison of experimental results with Mirels's formulations. In Mirels's model the flow properties are expressed as

$$M_2 = \frac{A_{2,s}}{A_2} M_{2,s} \left\{\frac{2 + (\gamma_2 - 1)M_2^2}{2 + (\gamma_2 - 1)M_{2,s}^2}\right\}^{(\gamma_2+1)/2(\gamma_2-1)} \tag{18}$$

A time-dependent M_2 for assumed values of $A_{2,s}/A_2$ is calculated by iter-

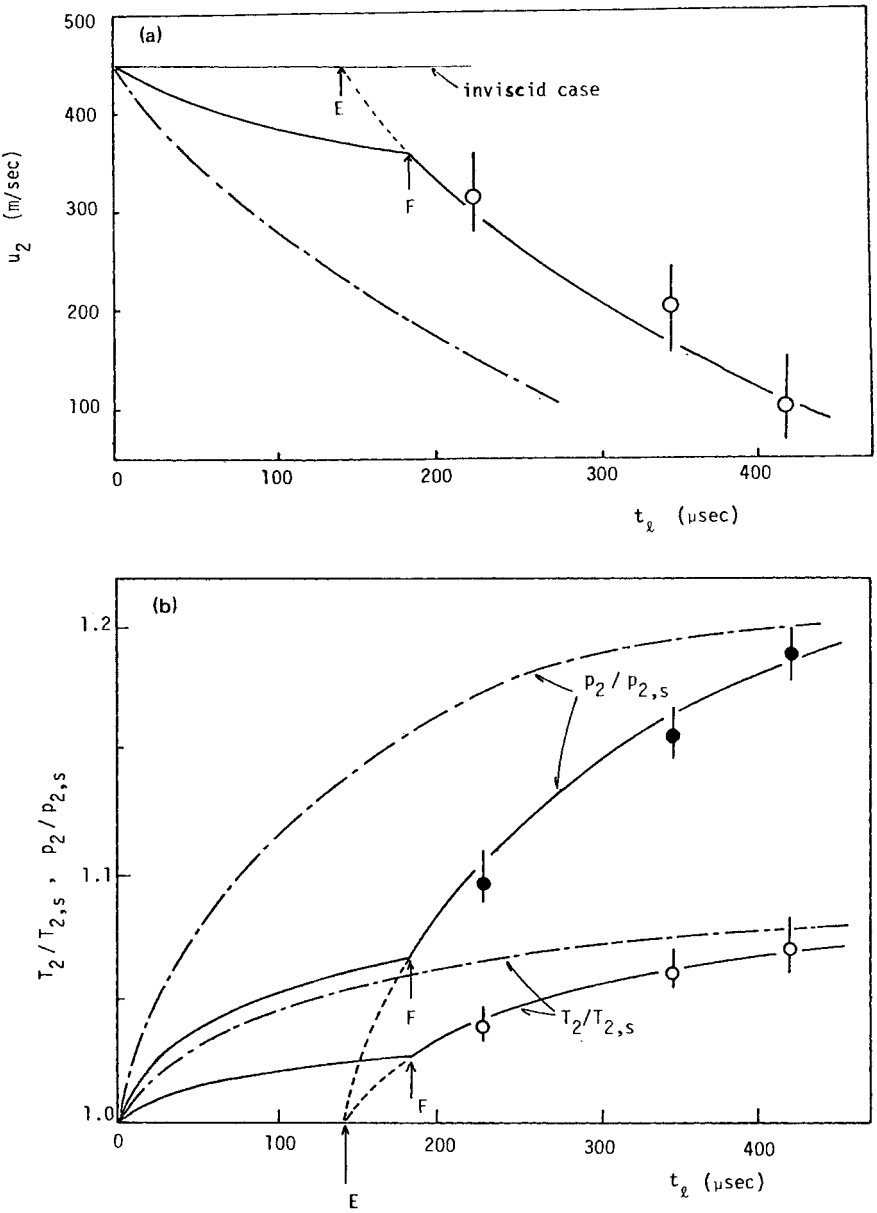

Figure 10. Variation of flow properties of argon, $p_1 = 30$ torr, $M_s = 5$, in the transition case. (a) Particle velocity relative to shock front. (b) Pressure and temperature. Marks are values obtained by a tracer experiment. Lines are calculated by Mirels's formulation: solid lines—transition model; chain lines—turbulent model. E shows the effective origin of turbulence, and F shows the transition point.

ation from eqs. (11) and (18). Using eq. (17), time-dependent values of T_2, P_2, and ρ_2 can be calculated from M_2. Comparison of the values thus calculated with those obtained from the tracer method shows good agreement, as shown in Figure 10.

Pressure profiles obtained by the piezo gauge and infrared emission profiles of nitric oxide are compared with those obtained using Mirels's model in Figure 11, where the transitions of the boundary-layer condition are observed. These results show that the correction for the boundary-layer effect by this model is satisfactory.

Boundary-Layer Effects on Chemical Kinetics

As described in the previous section, it may be considered that there are cases where the corrections of shock parameters are required in a chemical kinetic study. In this section some examples are given.

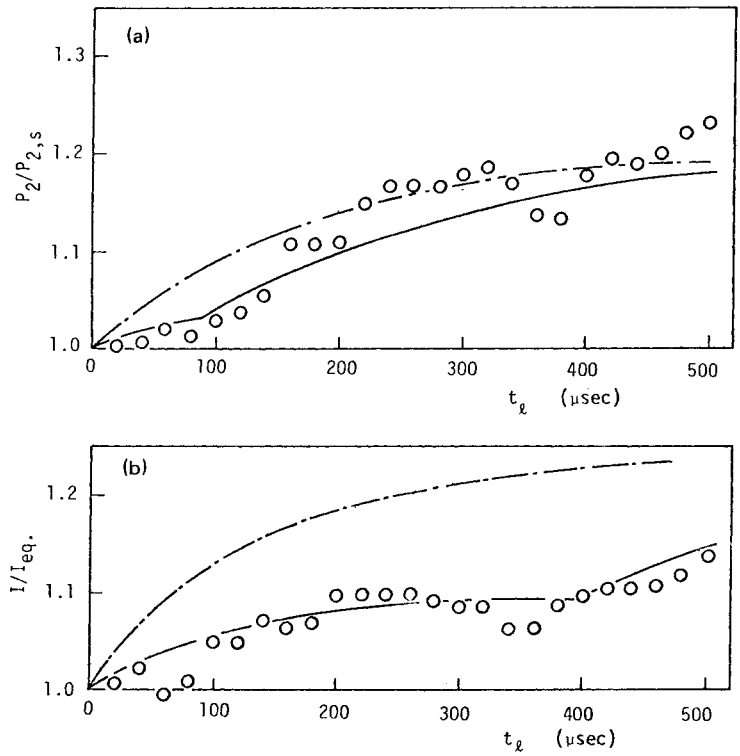

Figure 11. Comparison of profiles obtained experimentally with those calculated by the duct-flow model. Points are experimental values. Lines are calculated values: solid lines—transition model; chain lines—turbulent model. (a) Pressure profile. Test gas argon; p_1 = 150 torr; M_s = 4.3 [see Fig. 1(b)]. (b) Profile of emission of nitric oxide. Test gas $(NO)_0/(Ar)_0$ = 1/9; p_1 = 23 torr; M_s = 4.28 [see Fig. 1(c)].

Reaction time. The boundary-layer effect on the reaction time is most important. The further the gas particle is from the shock front, the more pronounced is the effect.

Figure 12 shows an Arrhenius plot of the decomposition rates of nitric oxide, $-d(\mathrm{NO})/dt$, obtained by the inviscid flow assumption and by the corrections described in this study. As explained in detail in [7], a previous estimation [8] of the reaction order of the decomposition of nitric oxide was erroneous and led to an incorrect conclusion.

Temperature and pressure rise. It is often observed in oscillograms of shock-tube experiments that the concentrations of reactants increase a little at the beginning periods of reaction. This fact is quite understandable according to the preceding explanation, as illustrated in Figure 13. The conversions of nitric oxide in the shock wave at $l/l_m = 0.01$ are plotted. At the point of constant l/l_m, $t_f/(t_1 \cdot \rho_{21})$ is constant, and $P_2/P_{2,s}$, $T_2/T_{2,s}$, and $\rho_2/\rho_{2,s}$ are almost constant, regardless of the initial pressure and shock Mach number. In Figure 13 computed values are shown also. These were obtained numerically by solving the kinetic equations, based on the mechanism of the nitric oxide decomposition [7], taking boundary-layer effects

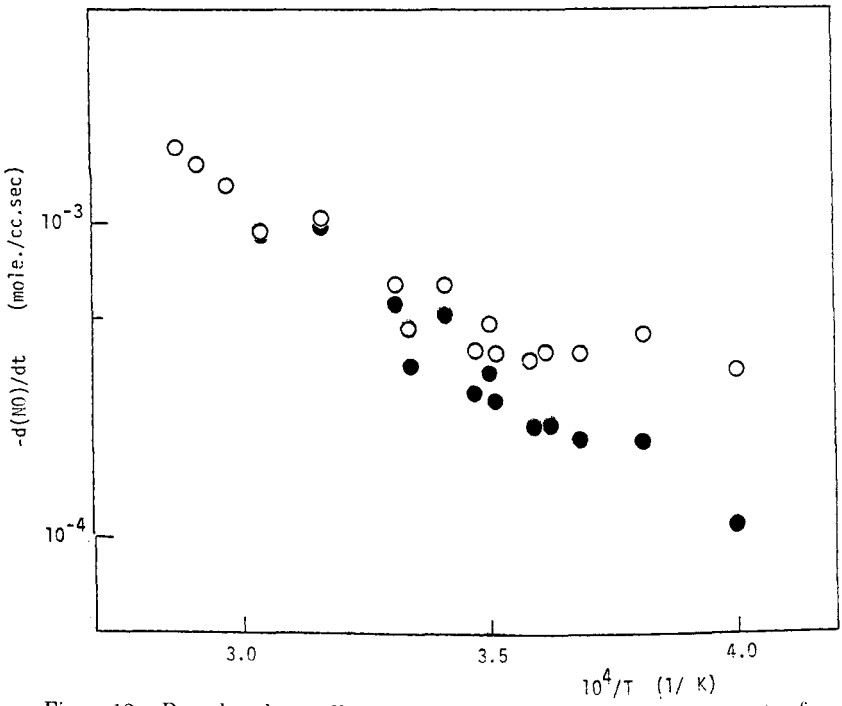

Figure 12. Boundary-layer effect on reaction time in the decomposition rate of nitric oxide at $(\mathrm{NO})/(\mathrm{NO})_0 = 0.8$. Test gas $(\mathrm{NO})_0/(\mathrm{Ar})_0 = 1/9$; $p_1 = 30$ torr. ○—inviscid treatment; ●—corrected values for reaction time.

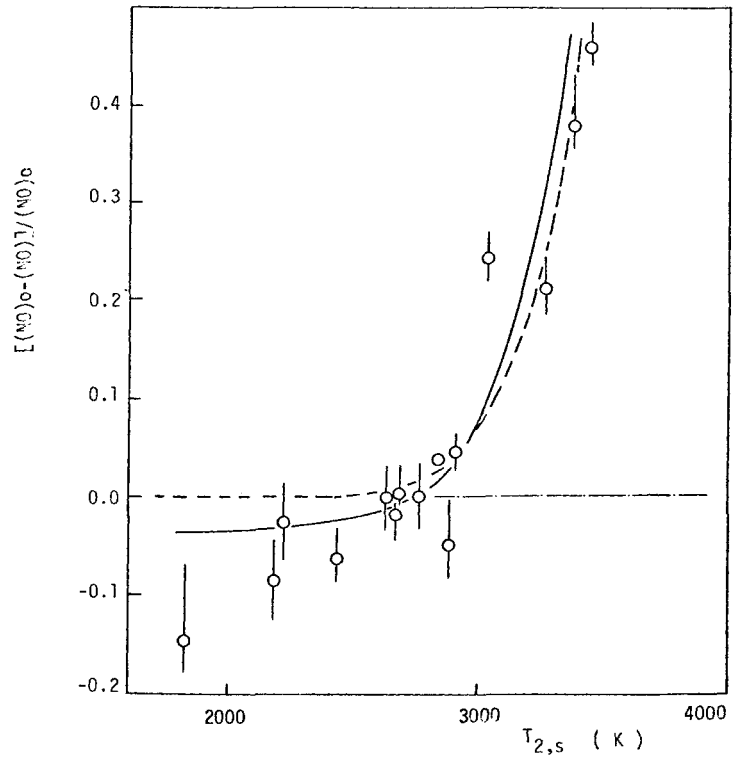

Figure 13. Boundary-layer effects on reaction rate of nitric oxide at $l/l_m = 0.01$. Test gas $(NO)_0/(Ar)_0 = 1/9$; $p_1 = 30$ torr. Circles are experiments. Lines are calculated values: solid line—laminar model; dashed line—inviscid model.

into account. Negative values of the rate of conversion do not have physical meaning. Accordingly, one must be careful in evaluating reaction rates from the initial slopes of concentration profiles.

Modeling calculations of chemical reaction in shock waves. Gardiner and co-workers [9] and Bittker and co-workers [2] made computer programs for numerical calculation of the progress of chemical reactions in incident shock waves, taking into account Mirels's model of boundary-layer effects. In their programs the boundary layer is treated as fully laminar or fully turbulent. In many cases, however, transition from laminar to turbulent in boundary layers occurs as shown above. Two methods may be considered to treat these cases.

First, as was done by Gardiner and co-workers and Bittker and co-workers, assuming isentropic flow, that is, that the chemical reactions do not influence the diverging duct of shock-gas flow, the shape of the duct is determined as follows. (a) The transition point is determined experimentally. (b) The two diverging ducts are connected by eq. (12). (c) The cross-sectional area of the ducts is calculated by the equations

$$A_2/A_{2,s} = \begin{cases} 1/[1 - (l/(l_m)_{lam})^{1/2}], & l < (l_t)_{lam} \quad (19a) \\ 1/[1 - \{(l - (l_t)_{lam} + (l_t)_{turb})/(l_m)_{turb}\}^{4/5}], & l > (l_t)_{lam} \quad (19b) \end{cases}$$

In Figure 5 of [7] an example of calculations done by this method is shown.

Second, the exact treatment can be considered, which removes the assumption of isentropic duct flow, that is, one solves eqs. (6)–(8) taking into account heats of reaction and changes of moles by reaction. However, this method seems to be infeasible due to tediousness. Usually, sample gas is highly diluted by an inert gas, such as argon, which suppresses these effects.

Conclusion

Boundary-layer effects in incident shock flow were studied experimentally. The results were as follows. (a) By the tracer method the boundary-layer effect on the particle time of flight could be obtained directly. (b) Profiles of temperature, pressure, and density behind the shock front could then be derived using the shock relations. (c) These results, which were obtained using nearly pure argon as test gas, could be extended to various gas mixtures. (d) Experiments were compared with Mirels's model, and it was concluded that the model is essentially sufficient to explain the experimental results. However, it is not appropriate to use the model to determine whether the shocked flow is in the laminar or the turbulent boundary-layer condition, since Mirels's formulations for the transition Reynolds number prove to be inaccurate.

There are several points left to be clarified, (a) whether Mirels's turbulent model is applicable to the case of high initial pressure and of high shock Mach number, as pointed out by previous investigators [4]; (b) what is the effect of shock attenuation on the properties of shocked flow, which has not been treated by Mirels or others [1,3]; (c) whether $t_1/(t_1)_i = \alpha_x$ can be treated as constant beyond the conditions examined in this study; (d) whether a more refined formulation of the transition Reynolds number can be found.

It is advisable to perform tracer experiments before carrying out a shock-tube study on chemical kinetics, since (a) they are not affected by the disturbance of the contact surface caused by the nonideal diaphragm rupture, and (b) there is no need to consider whether the boundary layer is laminar, turbulent, or in transient condition, so long as one deals with the particle time of flight, which has serious effects in the study of chemical kinetics using the shock tube.

Acknowledgment

This work was supported by Grant 911503 in Aid for Scientific Research from the Ministry of Education and the Fund of NO_x Elimination Technique from the Japan Iron and Steel Federation. The authors wish to express their thanks to Dr. I. Wada and Professor A. Takano for valuable discussions.

Bibliography

[1] H. Mirels, Proc. 8th Int. Shock Tube Symp., Chapman & Hall, London, 1971, paper 6; *Phys. Fluids,* **6,** 1201 (1963); *A.I.A.A.J.,* **2,** 84 (1963); *Phys. Fluids,* **9,** 1907 (1966).
[2] M. Warshay, *J. Chem. Phys.,* **54,** 4060 (1971); F. E. Belles and T. A. Brabbs, 13th (Int.) Comb. Symp., 1971, p. 129; D. A. Bittker and V. J. Schullin, NASA TN-D6585, 1972.
[3] W. C. Gardiner, Jr., M. McFarland, K. Morinaga, T. Takeyama, and B. F. Walker, Proc. 8th Int. Shock Tube Symp., 1971, paper 23; J. J. Bertin, E. S. Ehrhardt, W. C. Gardiner, Jr., and T. Tanzawa, Proc. 10th Int. Shock Tube Symp., 1975, p. 575.
[4] R. G. Fuehrer, Proc. 7th Int. Shock Tube Symp., 1969, p. 31; J. J. Lacey, *ibid.,* p. 126.
[5] H. Schlichting, "Boundary-Layer Theory," McGraw-Hill, New York, 1968.
[6] R. A. Hartunian, A. L. Russo, and P. V. Marrone, J. Aerospace Sci., **27,** 587 (1960).
[7] M. Koshi and T. Asaba, *Int. J. Chem. Kinet.,* **11,** 305 (1979).
[8] M. Koshi, H. Ando, M. Oya, and T. Asaba, 15th (Int.) Comb. Symp., 1974, p. 807.
[9] W. C. Gardiner, Jr., private communication.

Received May 24, 1978
Revised June 19, 1978